ELSEVIER

Spectrochimica Acta Part B xx (2005) xxx – xxx

SPECTROCHIMICA ACTA PART B

www.elsevier.com/locate/sab

Quantum efficiency improvement of a cesium based resonance fluorescence detector by helium-induced collisional excitation energy transfer

Tiffany L. Correll[a], Vlasta Horvatic[b,*], Nicoló Omenetto[a], Cedomil Vadla[b], James D. Winefordner[a]

[a]*Department of Chemistry, University of Florida, Gainesville, FL 32611, USA*
[b]*Institute of Physics, 10000 Zagreb, Croatia*

Received 24 March 2005; accepted 11 May 2005

Abstract

Quantum efficiency improvement of a cesium based resonance fluorescence detector (RFD) was achieved by enhancing the transfer in a particular channel of the RFD excitation scheme with noble gas-induced collisional excitation energy transfer (CEET). The influence of Cs–Ar and Cs–He collisional mixing between the 6D and 7P states in cesium on the quantum efficiency of the $6S \rightarrow 6D \rightarrow 7P \rightarrow 6S$ excitation scheme was investigated by fluorescence measurements at relevant transitions. Ar-induced CEET was found to have little effect on the fluorescence response and quantum efficiency of the Cs RFD excitation scheme. However, a 35 fold quantum efficiency increase in the cesium resonance fluorescence detector response at only moderate He pressures was observed.

Keywords: Resonance fluorescence detector; Atomic line filter; Energy transfer; Collision transfer; Cesium; Alkali–noble gas mixture

1. Introduction

Many optical techniques, including laser Doppler velocimetry, free space optical communication and chemical imaging can benefit from high spectral resolution photon detection. This detection is characterized by spectral discrimination of the order of GHz or MHz [1] (1 MHz corresponds to approximately 10^{-4} nm in the near-infrared region). Spectral resolution of this magnitude has recently been achieved by exploiting the narrow absorption features of gas phase atoms. Such absorption is intrinsically selective and can be monitored by detecting the fluorescence or ionization resulting from laser excitation coupled to selectively excited atomic states. Imaging can be accomplished by spatially expanding the excitation and/or ionization lasers into two dimensions. Fluorescence photons or electrical charges are only created and detected when the interrogated object emits or scatters radiation of an energy precisely matching one of the transitions of a pre-determined optimal excitation/ionization scheme.

Single-point photon detectors based on these concepts are called resonance ionization detectors (RIDs) and resonance fluorescence detectors (RFDs). In imaging mode, these devices are referred to as resonance ionization imaging detectors (RIIDs) and resonance fluorescence imaging detectors (RFIDs). Several versions of these devices have been described using mercury and cesium atoms [2–13].

The most recently developed atomic vapor fluorescence detector using Cs has been reported by Pappas et al. [8]. In this device, photons whose frequency falls within the narrow linewidth of the $6S_{1/2} \rightarrow 6P_{3/2}$ transition at 852.34 nm are imaged with a lens into the front of a Cs vapor cell and absorbed by the ground state atomic population. These signal photons can be the result of Doppler or Raman

* Corresponding author. Fax: +385 1 469 8889.
E-mail address: blecic@ifs.hr (V. Horvatic).

0584-8547/$ - see front matter © 2005 Elsevier B.V. All rights reserved.
doi:10.1016/j.sab.2005.05.001

frequency-shifted radiation. The resulting excited $6P_{3/2}$ state atoms are pumped to the $6D_{5/2}$ state by laser excitation at 917.47 nm. The sequentially excited atoms radiatively decay to the $7P_{3/2}$ level and subsequently generate fluorescence at 455.65 nm upon returning to the ground state via the $7P_{3/2} \rightarrow 6S_{1/2}$ transition. This wavelength-shifted fluorescence is detected optically and serves as the analytical signal indicative of the initial absorption event. Because fluorescence photons are detected or imaged only when a photon is absorbed in the first resonant transition, the spectral response of this imaging detector was initially limited by the Doppler-broadened linewidth of the 852.34 nm transition at the operating temperature of the detector, i.e., approximately 400 MHz or 9.7×10^{-4} nm at 852.34 nm and 298 K. The spatial resolution, limited by resonance radiation diffusion, was better than 200 μm [9].

The Doppler-broadened resonance fluorescence detector has been described as a method of detecting Mie scatter from a suspension of silica particles [10]. In addition, sub-Doppler spectral resolution in cesium fluorescence-based devices has been achieved through excitation of a monokinetic population of the $6P_{3/2}$ state by arrangement of the excitation lasers in either co-propagating or counter-propagating beam geometry. Improvements achieved by excitation of a selective population of atoms resulted in a sub-Doppler spectral resolution of 200 MHz or 0.5 pm at 852.34 nm for single-point detection with counter-propagating geometry [11]. A sub-Doppler spectral resolution of 270 MHz was also realized in the imaging mode, using co-propagating geometry. Improvements in experimental design, namely the addition of an image intensifier and cooled CCD camera, have resulted in an increased sensitivity of 10^8 photons per pixel [12]. Additional efforts have focused on demonstrating the use of the improved Cs RFD and RFID for moving object detection. In these studies, a rapidly rotating disk, illuminated by 852.34 nm radiation, was used to generate Doppler-shifted photons which were detected and imaged [13]. Velocity differences of 15 m/s could be resolved and a working detection range of up to 1500 m/s was available given the tuning characteristics of the first excitation laser.

Although cesium RFDs and RFIDs have demonstrated superior spectral resolution, the application of these devices is still limited due to low sensitivity when compared to high-gain devices with poor spectral resolution. In order to simultaneously improve the efficiency of the chosen two-step cesium RFD/RFID excitation scheme and minimize the occurrence of radiation trapping and image distortion, noble gas-induced collisional excitation energy transfer (CEET) between the cesium 6D and 7P states was investigated.

2. Experimental approach

2.1. Measurement procedure

Noble gas-induced $6D \rightarrow 7P$ collisional mixing in cesium was investigated in a stainless steel, crossed heat pipe oven as shown in Fig. 1. For the readers' convenience we mention that heat pipe ovens used in laser spectroscopy [14] are based on the heat conductive element initially designed by Grover, Cotter, and Erickson [15,16]. A traditional heat pipe is a hollow cylinder filled with a vaporizable liquid, also called a working fluid. This fluid is evaporated by an

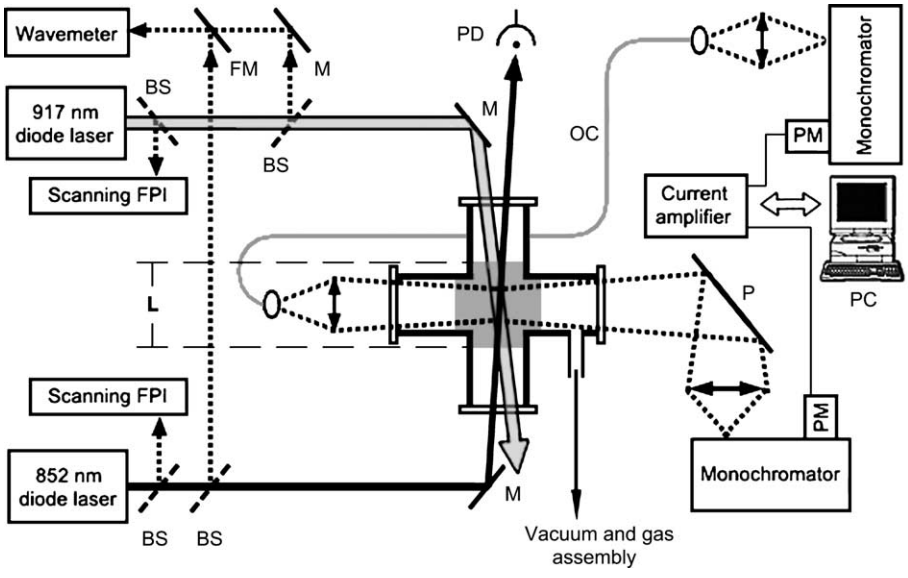

Fig. 1. Experimental setup used to conduct He and Ar-induced CEET studies in cesium. BS=beam splitter, FPI=Fabry–Perot interferometer, M=mirror, FM=flipping mirror, P=periscope, PM=photomultiplier, PD=photodiode, OC=optical cable and L=cesium vapor column length (equal along both heat pipe arms). Inclination of the laser beams inside the heat pipe is exaggerated.

external heat source at one end of the pipe. A heat sink, placed at the other end of the pipe, drives vapor down the tube where it condenses. In this way, the working fluid alternately evaporates and condenses, transferring heat from one region of the tube to another. The evaporation–condensation cycle is made possible by the use of a wick or capillary structure that lines the inner surface of the cylindrical wall and provides the driving force necessary to return the condensate to the evaporator. In this way, the device constantly generates a homogenous vapor which is continuously purified during operation.

In this experiment, the heat pipe oven was equipped with a centrally placed cross-shaped heater (cross length: 4.5 cm) and water-cooled quartz windows. A screen mesh lined the inner walls of the pipe. The heat pipe was filled with helium or argon as a buffer gas, and it was not running in the heat-pipe mode (mode in which the buffer gas pressure is equal to the pressure above the working liquid). The cesium vapor was confined within the volume having the equal linear dimension $L=(6\pm1)$ cm along the both heat pipe arms (see Fig. 1). To determine L, a thin tungsten wire was built in along the heat-pipe axis (thermionic diode configuration), and the heat pipe was heated to several temperatures covering the temperature range of operation. After each heating the wire was dismounted and inspected under the microscope. The segment which was attacked by alkali vapor as well as metal droplets deposited at the hot zone boundaries were clearly observable, enabling the determination of the metal vapor column length with the stated accuracy. No systematic variation of L with the change of the temperature was observed. In addition, a vacuum and gas assembly allowed the atmosphere in the pipe to be controlled.

The cesium atoms were excited from the ground state by the laser radiation from a single-mode laser diode (Qphotonics, model QLD-850-100S, $\lambda=850$ nm at 25 °C, maximum power 100 mW). The laser was tuned to excite the red wing of the $6S_{1/2}(F=4)\rightarrow 6P_{3/2}(F)$ hyperfine transition. Cesium atoms in the $6P_{3/2}$ state were further excited to the $6D_{5/2}$ state by a counter-propagating laser beam, which was provided by another single-mode laser diode (Qphotonics, model QLD-820-100S, $\lambda=918$ nm at 25 °C, maximum power 100 mW) centered on $6P_{3/2}\rightarrow 6D_{5/2}$ transition. Both diodes were mounted on Peltier elements inside custom-built diode laser housings. Operating current and temperature was controlled by commercial diode laser drivers (PROFILE Optische Systeme GmbH, model ITC 502).

Both laser beams were collimated (diameter: 2 mm) and had bell-shaped power distribution across the beam. The beams were overlapped along the whole length of the heat pipe. Each beam was split into three parts. One portion of the beam was directed through the focusing optics of a home-built, confocal 2 GHz free spectral range scanning Fabry–Perot interferometer (FPI). Transmission peaks of the FPI were used to calibrate the absorption spectra as well as to control single-mode operation of the laser diodes. In addition, a fraction of the beam was overlapped for approximately 1 m with the He–Ne reference beam of a commercial wavemeter (Burleigh Instruments Inc, model WA-20VIS) and used for wavelength determination. The majority of each beam was directed through the input windows of the heat pipe oven containing cesium. The powers of the laser beams transmitting the heat-pipe entrance window were measured by power meter (Coherent, model Filedmaster LM-2). Typical powers of the 852 and 917 nm diode laser beams were 19 and 9 mW, respectively.

The experimental arrangement also allowed for the measurement of the unsaturated ground state absorption. The absorption measurements were performed by manual temperature tuning of the 852 nm diode laser across the $6S_{1/2}\rightarrow 6P_{3/2}$ transition. For that purpose the laser power was reduced down to ~10 μW using neutral density filters. The transmitted radiation was detected by a photodiode and the confocal FPI was used to calibrate the dispersion of the spectrum. Absorption coefficient obtained from the measured spectra was used for the determination of the cesium ground-state number density. The temperature of the cesium vapor was subsequently obtained using the vapor pressure curve of cesium [17,18].

Two monochromators were used to measure fluorescence intensities of the spontaneous emission at $6D_{3/2,\,5/2}\rightarrow 6P_{3/2}$ (921 and 917 nm lines) and $7P_{1/2,\,3/2}\rightarrow 6S_{1/2}$ (459 and 455 nm lines) transitions. The fluorescence observed emerged from the region ~1 cm long in the middle of the heated zone. The simultaneous imaging of the cylindrical fluorescence zone onto the entrance slits of the monochromators is depicted in Fig. 1. On one side the fluorescence was collected with mirrors arranged as a periscope and focused onto the entrance slit of a 0.5 m monochromator (Jarrell-Ash, model 82025) equipped with a Peltier-cooled photomultiplier (model RCA 7102, S1 cathode) used to measure 917 and 921 nm fluorescence. With 150 μm slits the resolution of the Jarrell-Ash monochromator was 0.8 nm. Through the opposite window the fluorescence was collected by the use of slit-type fiber optic bundle. For the collection and detection of the radiation, the fiber optic bundle was coupled via a lens to a 1 m monochromator (McPherson, model 2051) used for 455 and 459 nm signal measurements. This monochromator was supplied with an S11 cathode photomultiplier (model EMI 9524S) and its resolution was 0.1 nm with 80 μm slits.

A relationship between the signals measured by the two fluorescence detection systems was determined in the following way. Under the conditions where the blue fluorescence signals were the largest (He pressure of ~10 mbar), the 455 and 459 nm intensities were measured simultaneously with the McPherson/PMT arrangement and the Jarrell-Ash/PMT assembly. Comparison of these

signals allowed a calibration to be established between the two detection systems. At all other He pressures in the investigated range (0.25–12.2 mbar), the blue fluorescence intensities measured with McPherson/PMT arrangement were reported in terms of the Jarrell-Ash/PMT response using the obtained calibration factor. In addition, all signals were corrected for the responsivity of the Jarrell-Ash/PMT system which was measured with a calibrated tungsten-ribbon lamp (PHILIPS model W2KGV22i).

At helium pressures of 0.5, 2, and 12.2 mbar, monochromator scans were recorded. The PMT output was amplified (Model Keithley 616) and sent to a digital voltmeter (Model Keithley 196) interfaced to computer via a GPIB card (Model 183617K-01, National Instruments). Data was acquired using Labview software (Version 6.1, National Instruments).

2.2. Determination of the relative number densities in the excited cesium states

The partial energy level diagram of cesium including the transitions pertinent to this study is shown in Fig. 2. In addition, the wavelengths, oscillator strengths and spontaneous emission rates associated with these transitions can be found in Table 1. To evaluate the effect of He and Ar-induced 6D→7P collisional mixing on the fluorescence response of the RFD, the ratio of total 7P (N_{7P}) to total 6D (N_{6D}) population was measured as a function of He pressure. This population ratio (N_{7P}/N_{6D}) was determined by measurement of relative fluorescence intensities.

The fluorescence intensities of the optically thin lines arising in the $7P_{3/2}\rightarrow 6S_{1/2}$, $7P_{1/2}\rightarrow 6S_{1/2}$, $6D_{5/2}\rightarrow 6P_{3/2}$ and $6D_{3/2}\rightarrow 6P_{3/2}$ transitions, observed by a monochromator with large band-pass (0.1 and 0.8 nm in the present case) in comparison with the width of the lines, are spectrally integrated over the frequencies within the whole line profile. Therefore, the total fluorescence intensities I of

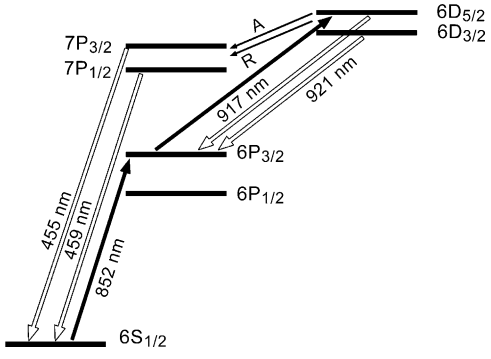

Fig. 2. Partial energy level diagram of cesium depicting the laser pumped transitions at 852 and 917 nm and the fluorescence intensities measured at 917, 921, 455, and 459 nm. Weak radiative transitions 6D→7P are indicated with rate A, while R labels collisional transfer rate due to Cs-noble gas collisions.

Table 1
The wavelengths λ, oscillator strengths f and spontaneous emission rates A of the transitions involved in the determination of the cross-section for the 6D→7P excitation energy transfer in cesium due to collisions with noble gas

No.	Transition	λ(nm)	f	A (10^7 s^{-1})
1	Cs ($6D_{5/2}$)→Cs ($6P_{3/2}$)	917.475	0.313[a]	1.65
2	Cs ($6D_{3/2}$)→Cs ($6P_{3/2}$)	921.104	0.0363[a]	0.283
3	Cs ($7P_{3/2}$)→Cs ($6S_{1/2}$)	455.650	0.0109[a]	0.17
4	Cs ($7P_{1/2}$)→Cs ($6S_{1/2}$)	459.439	0.00248[a]	0.079
5	Cs ($6D_{3/2}$)→Cs ($7P_{1/2}$)	12147	0.327[b]	0.0064
6	Cs ($6D_{3/2}$)→Cs ($7P_{3/2}$)	15570	0.032[b]	0.0009
9	Cs ($6D_{5/2}$)→Cs ($7P_{3/2}$)	14595	0.309[b]	0.0074

Spontaneous emission coefficients were calculated using the corresponding oscillator strength f of the transition.
[a] Values from [19].
[b] Values from [20].

the 455, 459, 917 and 921 nm lines emerging from the observation volume can be expressed as:

$$I_{455} \propto h\nu_{455} \cdot A_{455} \cdot N_{7P_{3/2}} \tag{1}$$

$$I_{459} \propto h\nu_{459} \cdot A_{459} \cdot N_{7P_{1/2}} \tag{2}$$

$$I_{917} \propto h\nu_{917} \cdot A_{917} \cdot N_{6D_{5/2}} \tag{3}$$

$$I_{921} \propto h\nu_{921} \cdot A_{921} \cdot N_{6D_{3/2}} \tag{4}$$

where A_i (i=455, 459, 917 and 921) denotes the spontaneous emission coefficient for transition at corresponding wavelength, while N_j (j=$7P_{3/2}$, $7P_{1/2}$, $6D_{5/2}$ and $6D_{3/2}$) labels the population of the initial level.

The ratio of the total populations in the 7P and 6D states of cesium can be represented by:

$$\frac{N_{7P}}{N_{6D}} = \frac{N_{7P_{3/2}} + N_{7P_{1/2}}}{N_{6D_{5/2}} + N_{6D_{3/2}}} = \frac{N_{7P_{1/2}}\left(1 + \frac{N_{7P_{3/2}}}{N_{7P_{1/2}}}\right)}{N_{6D_{3/2}}\left(1 + \frac{N_{6D_{5/2}}}{N_{6D_{3/2}}}\right)}. \tag{5}$$

Therefore, from Eqs. (1)–(5) it follows:

$$\frac{N_{7P}}{N_{6D}} = \frac{I_{459} \cdot \lambda_{459} \cdot A_{921}}{I_{921} \cdot \lambda_{921} \cdot A_{459}} \cdot \frac{\left(1 + \frac{I_{455} \cdot \lambda_{455} \cdot A_{459}}{I_{459} \cdot \lambda_{459} \cdot A_{455}}\right)}{\left(1 + \frac{I_{917} \cdot \lambda_{917} \cdot A_{921}}{I_{921} \cdot \lambda_{921} \cdot A_{917}}\right)}. \tag{6}$$

Referring to Table 1, upon simplification, Eq. (6) yields:

$$\frac{N_{7P}}{N_{6D}} = 1.79 \cdot \frac{I_{459}\left(1 + 0.46 \cdot \frac{I_{455}}{I_{459}}\right)}{I_{921}\left(1 + 0.17 \cdot \frac{I_{917}}{I_{921}}\right)}. \tag{7}$$

The pumping in the center of the nearly pure Doppler profile is velocity selective, and even in the case of strong saturation of the considered velocity group the number density of the atoms realized in the excited state is small

compared with the density of the ground-state atoms [21]. In the separate experiment [22], the Cs 6P and 6D populations created by $6S_{1/2} \rightarrow 6P_{3/2} \rightarrow 6D_{5/2}$ excitation in the center of optically thin Doppler lines were investigated in dependence on the pump power applied in each excitation step. It was found that under the conditions of the saturation of the selected velocity group in the $6S_{1/2} \rightarrow 6P_{3/2}$ transition, the $6P_{3/2}$ state population produced amounted to only $\approx 2\%$ of the ground-state density. The experimentally determined populations in the $6P_{3/2}$ state were found to be in excellent agreement with the ones calculated using the appropriate expressions given in [21]. In the present experiment, the profile of the $6S_{1/2} \rightarrow 6P_{3/2}$ line was generally of Voigt type (the ratio of the Lorentz and Doppler widths $a = \Delta_L/\Delta_D$ varied from 0.025 to 1.04 in the range of the applied He pressures) and the transition was optically thick. Therefore, the pumping was done in the optically thin Lorentzian wing of the line at detunings of about 1 GHz from the line center. Depending on the $6S_{1/2} \rightarrow 6P_{3/2}$ line pressure broadening, the pump detuning was optimized so as to maximize 917 nm signal for the particular He pressure. By applying the calculation given in [21] to the present experimental conditions, we have determined that the highest excited $6P_{3/2}$ state population achieved was on the order of 10^7 cm^{-3}. The $6P_{3/2} \rightarrow 6D_{3/2,5/2}$ transitions were completely optically thin, and therefore, there was no need to correct the measured 917 and 921 nm fluorescence intensities for the absorption at the optical path r corresponding to the radial dimension of the fluorescence zone ($r \approx 0.1$ cm).

The transition $6S_{1/2} \rightarrow 7P_{1/2,3/2}$ was slightly optically thick at the exit optical path $L/2$ and the observed 455 and 459 nm fluorescence signals had to be corrected for the corresponding absorption. The fluorescence intensity $I^{em}(\nu)$ emitted from the optically thin fluorescence zone is characterized by a line profile $P(\nu)$, i.e., $I^{em}(\nu) \propto P(\nu)$. At the path $\tilde{L}=L/2$ it is absorbed according to the Beer's law, and the intensity $I^{trans}(\nu)$ which is transmitted through the absorbing layer is given by $I^{trans}(\nu) = I^{em}(\nu) \times \exp[-KP(\nu)] \propto P(\nu) \times \exp[-KP(\nu)]$. Because all measured fluorescence intensities were spectrally integrated over the frequencies within the whole line profile due to large bandpass of the detection system, the measured intensity I^{meas} is related to the relevant I emerging from the fluorescence zone in the following way:

$$I^{meas} = I \cdot \xi \tag{8}$$

where ξ is the correction factor for the absorption on the path $\tilde{L}=L/2$, given by:

$$\xi = \frac{\int_{-\infty}^{\infty} P(\nu) \cdot e^{-K \cdot P(\nu)} d\nu}{\int_{-\infty}^{\infty} P(\nu) d\nu}. \tag{9}$$

In the above equation, $K = \pi e^2 N_{Cs} f \tilde{L}/mc$, where N_{Cs} is the cesium ground state number density. In the present case the line profiles were essentially of the Voigt type, and $P(\nu)$ in dimensionless form and normalized to unity in the line center is given by:

$$P(\nu) = \frac{2}{\pi \cdot \Delta_L} \cdot f_V(\nu, a) \tag{10}$$

where the Voigt function $f_V(\nu, a)$, is defined as:

$$f_V(\nu, a) = \frac{1}{4\sqrt{\pi}} \int_{-\infty}^{+\infty} \exp(-x^2) \times \frac{a^2}{\left(\nu - x/2\sqrt{\ln 2}\right)^2 + (a/2)^2} dx. \tag{11}$$

For the measurements at each helium pressure (i.e., for each value of $a = \Delta_L/\Delta_D$) the corresponding correction factor ξ was obtained by numerical integration. The correction for the absorption was made separately for each hyperfine component of the $6S_{1/2} \rightarrow 7P_J$ transition, and the total correction factor is obtained as $\xi = (f_{weak} \cdot \xi_{weak} + f_{strong} \cdot \xi_{strong})/(f_{weak} + f_{strong})$.

The intensities I_{917} and I_{921} appearing in Eq. (7) are related to the measured ones by $I_{917} = I_{917}^{meas}/\varepsilon_{917}$ and $I_{921} = I_{921}^{meas}/\varepsilon_{921}$, where I_{917}^{meas} and I_{921}^{meas} are the signals detected with Jarrell-Ash monochromator, while ε_{917} and ε_{921} denote the spectral responses of the Jarrell-Ash detection system at the respective wavelength. The blue fluorescence signals are given by $I_{455} = I_{455}^{meas} c_{455}/(\varepsilon_{455} \cdot \xi_{455})$ and $I_{459} = I_{459}^{meas} c_{459}/(\varepsilon_{459} \cdot \xi_{459})$, where I_{455}^{meas} and I_{459}^{meas} are the signals measured with McPherson arrangement, ξ_{455} and ξ_{459} are the He-pressure dependent correction factors for the absorption of the blue fluorescence on the optical path $L/2$, c_{455} and c_{459} label the calibration factors connecting the two detection systems (see Section 2.1), while ε_{455} and ε_{459} are the spectral responses of the Jarrell-Ash system at the corresponding wavelengths.

2.3. Determination of the cesium ground-state number density

The ground state cesium density N_{Cs} needed for the evaluation of the correction factor ξ, has been determined from the measurement of the absorption coefficient $k(\Delta\nu)$ in the wing of the cesium D2 line. In particular, the blue wing of the weak ($6S_{1/2}$ ($F=3$) $\rightarrow 6P_{3/2}$) and the red wing of the strong ($6S_{1/2}$ ($F=4$) $\rightarrow 6P_{3/2}$) hyperfine component of the D2 line were evaluated. Absorption measurement used for the N_{Cs} determination was obtained at a He pressure of 12.2 mbar (see Fig. 3a). At this pressure the line wings were sufficiently pronounced to enable reliable analysis. The $k(\Delta\nu)$ could be accurately determined at detunings $\Delta\nu$ from the center of each hyperfine component which fall within the impact region (3 GHz $< \Delta\nu <$ 6 GHz), where k exhibits the usual Lorentzian form [23] (see Fig. 3b):

$$k(\Delta\nu) = \frac{\pi e^2}{mc} \cdot f \cdot N_{Cs} \cdot \frac{\Gamma}{2\pi(\Delta\nu)^2} \tag{12}$$

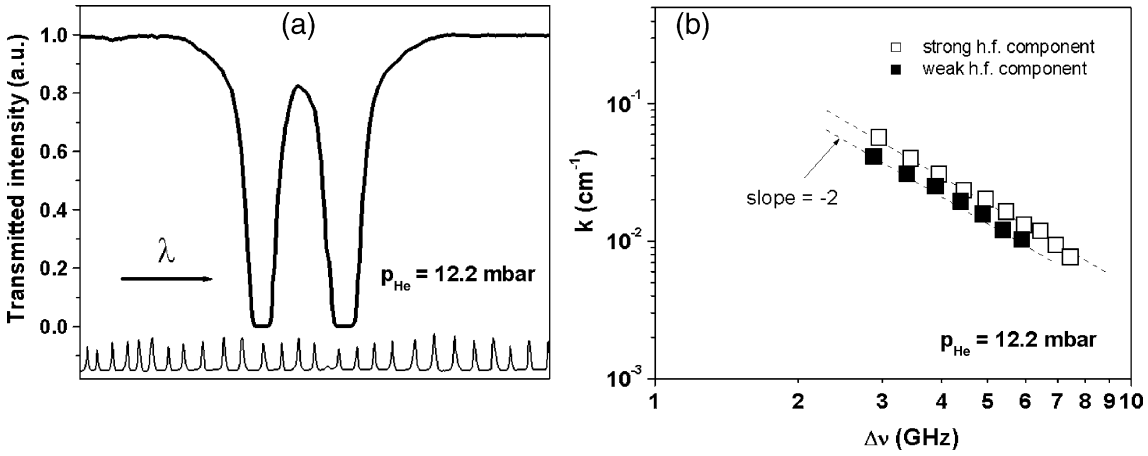

Fig. 3. (a) The unsaturated $6S_{1/2} \rightarrow 6P_{3/2}$ absorption measurement at 852 nm. The outer wings of the hyperfine components were used to determine ground-state cesium number density. The transmission peaks of the confocal Fabry–Perot interferometer with free spectral range of 2 GHz were used to calibrate the spectrum. (b) A plot of absorption coefficient versus detuning from the center of the particular hyperfine component into the outer wing. The plot demonstrates the Lorentzian nature of the line shape, i.e., the result is a straight line with a slope of −2 in accordance with Eq. (12).

where Γ is the half-width (FWHM) of the Lorentzian profile and f is the oscillator strength of the particular hyperfine component of the cesium D2 line, while the remaining symbols have their customary meaning. The absorption scan used for the N_{Cs} determination was measured in the presence of He as a buffer gas and the half-width Γ is therefore given by:

$$\Gamma = \Gamma_N + \Gamma_{Cs-He} + \Gamma_{Cs-Cs} \tag{13}$$

where Γ_N is the natural half-width, while Γ_{Cs-He} and Γ_{Cs-Cs} are the half-widths due to the Cs–He and Cs–Cs broadening, respectively. The half-widths Γ_{Cs-He} and Γ_{Cs-Cs} can be expressed in the form:

$$\Gamma_{Cs-He} = \gamma_{Cs-He} \cdot N_{He} \tag{14}$$

and

$$\Gamma_{Cs-Cs} = \gamma_{Cs-Cs} \cdot N_{Cs} \tag{15}$$

where γ_{Cs-He} and γ_{Cs-Cs} are the reduced half-widths for Cs–He and Cs–Cs broadening, respectively, and N_{He} is the number density of the helium atoms.

Because the heat-pipe was not working in the heat-pipe mode, the vapor in the central, heated zone, constituted a Cs–He mixture. Following the Dalton law, the total pressure in the warm zone was $p = p_{Cs} + p_{He}$, where p_{Cs} and p_{He} were the partial pressures of cesium and helium. Therefore, the helium number density in the middle of the heat-pipe is given by:

$$N_{He} = \frac{p}{k_B T} - N_{Cs} \tag{16}$$

where p is the pressure measured by manometer at the cold end (room temperature) of the system, k_B is the Boltzman constant and T is the temperature in the central zone of the heat-pipe.

By combination of Eqs. (12)–(16), we obtain the following quadratic equation:

$$(\gamma_{Cs-Cs} - \gamma_{Cs-He}) \cdot N_{Cs}^2 + \left(\Gamma_N + \gamma_{Cs-He}\frac{p}{k_B T}\right) \cdot N_{Cs} - k\frac{2mc}{f e^2}(\Delta\nu)^2 = 0 \tag{17}$$

the solution to which yields the value of the ground-state Cs density N_{Cs}, provided that temperature T in the central heated zone of the heat-pipe is known. Since this was not the case, Eq. (17) was solved iteratively using the room temperature T_0 in the first iteration step. The value $N_{Cs}^{(0)}$ obtained by solving the above equation for $T_0 = 293$ K and the vapor pressure curve of cesium [17,18] was then used to determine the temperature T_1 corresponding to $N_{Cs}^{(1)}$ density. This temperature was then used as an input parameter in the next iteration step. The iteration procedure converged in three steps, yielding the final values of N_{Cs} and T. Following the described procedure, the ground state Cs density was obtained for a series of discrete k values along the outer wings of the hyperfine components of the D2 line. The results are shown in Fig. 4. The cesium ground-state number density and temperature of the vapor were found to be $N_{Cs} = 3 \times 10^{12}$ cm^{-3} and $T = 350$ K, respectively.

Numerical values of the quantities appearing in Eq. (17) which were used in the evaluation are the following. For the Γ_N we have used the value 5.18 MHz [19]. Values for the broadening parameters $\gamma_{Cs-He} = (3.6 \pm 0.5) \times 10^{-10}$ s^{-1} cm^3 (obtained at $T = 503$ K) and $\gamma_{Cs-Cs} = (6.7 \pm 1) \times 10^{-7}$ s^{-1} cm^3 (measured at $T = 298$ K) were taken from [24] and [25], respectively.

According to theory, [26], the self-broadening parameter γ_{Cs-Cs} does not depend on temperature, while the γ_{Cs-He}

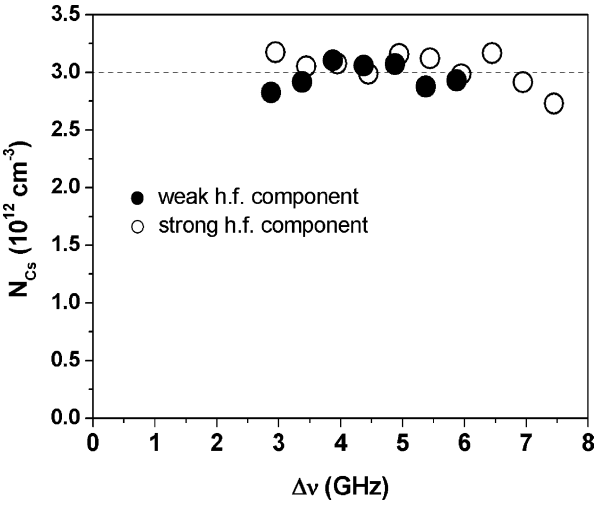

Fig. 4. Ground state cesium number density calculated according to Eq. (17) for several detunings in the outer wings of the hyperfine components of the 852 nm resonance line.

due to foreign-gas van der Waals' broadening exhibits a weak temperature dependence ($\sim T^{0.3}$). The vapor temperature in the present experiment was about 150 K lower than in [24] and the correction of γ_{Cs-He} for temperature dependence would amount to $\approx 10\%$. Since this correction is smaller than the error bar of the reported γ_{Cs-He} value it was neglected in the evaluation. As for the oscillator strengths of the hyperfine components of the Cs D2 line, we have used the values $f_{weak}=0.310$ and $f_{strong}=0.398$ [21]. As can be seen from Eq. (17), main contributions to the overall error bar of the N_{Cs} are due to the uncertainty in the experimentally determined quantity k, and the quantities γ_{Cs-Cs} and γ_{Cs-Cs} taken from literature. The error in determination of the absorption coefficient k is mainly due to the error in vapor-column length determination and amounts to ±17%. The variation of the k within its error bar produces the uncertainty in the N_{Cs} of ±14%. Analogously, variation of γ_{Cs-Cs} and γ_{Cs-He} within their error bars resulted with change of N_{Cs} value of less than ±1% and ±12%, respectively. With all sources of the uncertainties taken into account by adding errors in quadrature, the N_{Cs} was determined with an overall standard error of ±20%.

3. Results and discussion

Recent [21] theoretical considerations which proposed that the quantum efficiency of the Cs RFD excitation scheme could be significantly improved with collisional excitation energy transfer were tested experimentally by performing measurements in Cs–Ar and Cs–He mixtures. Argon as a buffer gas inducing 6D-7P inter-multiplet mixing is more than two orders of magnitude less effective than helium (see cross-section data in [21]) and in the present case it was chosen to create the experimental conditions which, according to the prediction [21], should closely resemble the pure cesium vapor.

The fluorescence spectra of 917, 921, 455 and 459 nm lines recorded in Ar and He at comparable pressures are shown in Fig. 5. All other relevant parameters (Cs ground-state density, pump powers in both excitation steps, etc.) were the same in both measurements. As can be seen from

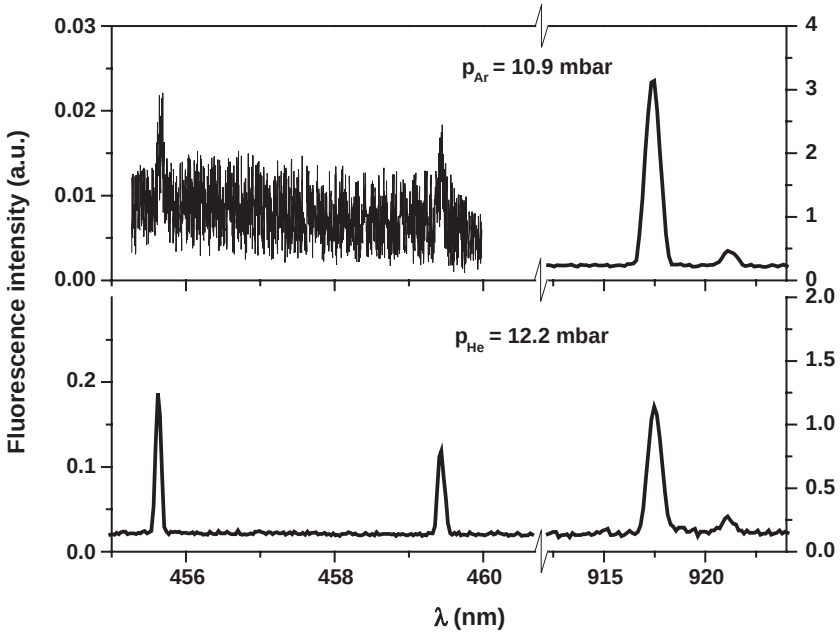

Fig. 5. Monochromator scans of fluorescence spectra of 917, 921, 455, and 459 nm lines obtained in Ar and He for comparable pressures. The displayed intensities are corrected for the spectral response. The correction of the blue fluorescence spectra for the absorption on the optical path towards the exit window is not included. The absorption-correction factors ξ for the peak intensities I_{455} and I_{459} in Ar and He, in the present experimental conditions amount to $\xi_{455}^{Ar}=0.455$, $\xi_{459}^{Ar}=0.846$, $\xi_{455}^{He}=0.675$, $\xi_{459}^{He}=0.908$.

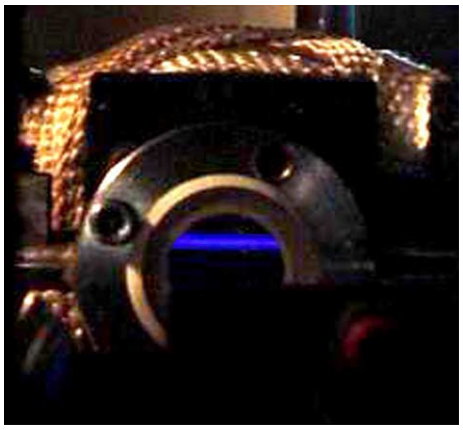

Fig. 6. Blue fluorescence observed at 7P→6S transition in the Cs–He mixture at cesium ground state density $N_{Cs}=3\times10^{12}$ cm^{-3}, and He pressure of 12.2 mbar. Photo was taken through the heat-pipe side-window by digital camera.

the Fig. 5, the blue fluorescence signals observed in Ar are just above the noise level, while in helium they are about 20 times larger. The exact amount of the enhancement can be calculated using Eq. (7) and taking into account the correction for the absorption of the blue fluorescence on the optical path $L/2$. The calculation yields the population ratios $(N_{7P}/N_{6D})_{Ar}=0.04$ and $(N_{7P}/N_{6D})_{He}=1.4$, which show that the population in the 7P state relative to the population in the 6D state is enlarged by a factor of 35 in the presence of helium.

The obtained results have shown that Ar-induced CEET has little effect on the fluorescence response and quantum efficiency of the Cs RFD excitation scheme. Furthermore, at 350 K, the presence of any Ar-induced effect may be masked by collisional excitation energy transfer induced by collisions with cesium ground state atoms. On the other hand, the blue fluorescence enhancement by He induced 6D-7P inter-multiplet mixing was so intense that the radiation could be seen by naked eye as shown in Fig. 6. These results represent experimental confirmation of the previous theoretical predictions [21].

Fluorescence intensities measured at 455, 459, 917 and 921 nm as a function of He pressure in the range between 0.25–12.2 mbar, are shown in Fig. 7.

The $6P_{3/2}$ state was populated from the ground state by pumping the strong hyperfine component of the $6S_{1/2}\rightarrow6P_{3/2}$ transition in the optically thin region of the red wing at a detuning of $\Delta\nu\approx1$ GHz from its center. The frequency of the laser in the upper excitation step $6P_{3/2}\rightarrow6D_{5/2}$ was adjusted to meet the condition for the two-step $6S_{1/2}\rightarrow6D_{5/2}$ excitation. The pumping powers in the first (852 nm) and the second (917 nm) excitation steps were 19 and 9 mW, respectively. At each He pressure the frequencies of both lasers were optimized to produce maximum fluorescence on the $6D_{3/2,\,5/2}\rightarrow6P_{3/2}$ transition.

During the measurements at different He pressures the population in $6P_{3/2}$ state was checked by taking the monochromator scan of the fluorescence at $6P_{3/2}\rightarrow6S_{1/2}$ transition. At constant ground-state Cs density the intensity in the quasistatic resonance wing (I_{852}^{wing}) of the line reflects the population in the excited state, and it was used to monitor the population of $6P_{3/2}$ level. The intensity of the optically thin quasistatic blue wing of the cesium D2 line emitted at the detuning $\Delta\nu$ from the line center is $I_{852}^{wing}(\Delta\nu)\propto A_{852}^{\nu}N_{6P_{3/2}}$, where A_{852}^{ν} is detuning dependent spectral emission coefficient [27,28]. If the reading of the wing intensity is taken at detuning $\Delta\nu$ which is large compared with monochromator band-pass the spectral emission coefficient A_{852}^{ν} can be regarded constant within the interval $\delta\nu$. Thus, by comparing the I_{852}^{wing} intensities at certain detunings measured at different He pressures it was found that the population in the $6P_{3/2}$ state did not change significantly with increasing He pressure. This observation is plausible bearing in mind that the $6S_{1/2}\rightarrow6P_{3/2}$ pumping was done in the Lorentzian wing of the Voigt profile, and in that case the excited state population $N_{6P_{3/2}}\propto\Pi_{01}^{eff}/A_{10}^{eff}$[21]. The effective pump rate Π_{01}^{eff} (at some constant pump detuning) increases as the profile of the line widens [21], but this gain is cancelled out by the simultaneous increase of the effective spontaneous emission rate.

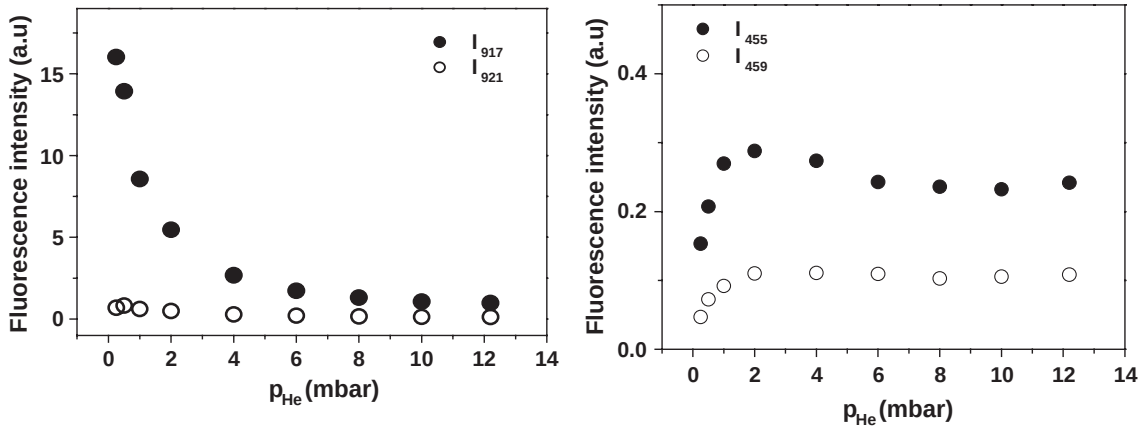

Fig. 7. The peak fluorescence intensities at 917, 921, 455 and 459 nm as a function of helium pressure. In the displayed data all necessary corrections of the measured intensities (see Section 2.2) are taken into account.

Fig. 7 shows that 917 and 921 fluorescence decreases with increasing He pressure, while the blue fluorescence signals (455 and 459 nm) increase and then level-off. The total population in 7P and 6D states (expressed in arbitrary units) is given by:

$$N_{7P}+N_{6D}\alpha\left(\frac{I_{917}}{v_{917}\cdot A_{917}}+\frac{I_{921}}{v_{921}\cdot A_{921}}+\frac{I_{455}}{v_{455}\cdot A_{455}}+\frac{I_{459}}{v_{459}\cdot A_{459}}\right). \quad (18)$$

The dependence of $(N_{7P}+N_{6D})$ on helium pressure is shown in Fig. 8a. As one can see, the total population in these states is almost constant (within the experimental error) in the range of He pressures above 2 mbar. The variation at the pressures <2 mbar can be ascribed partly to the difference between populations realized in the $6P_{3/2}$ state, and partly to the polarization of the 917 nm radiation which was not taken into account. All other fluorescence intensities used in the evaluation originate from the collisionally populated levels and are spatially isotropic. The 917 nm fluorescence was checked against polarization effects and they were found to be negligible for He pressures higher than 2 mbar. Therefore, from the results depicted in Fig. 8a it can be concluded that the observed decrease of the 917 and 921 nm fluorescence with increasing He pressure, occurs dominantly at the expense of increased population in the 7P state. The relative population N_{7P}/N_{6D} was calculated using Eq. (7), and displayed in Fig.(8b) as a function of He pressure. It can be seen that the response of the investigated RFD scheme substantially increases in the presence of He gas at moderate pressure.

The error bars plotted in Fig. 8 represent the total relative error in the determination of the quantities $(N_{7P}+N_{6D})$ and N_{7P}/N_{6D}, which includes the uncertainties in the measurements of the fluorescence intensities and the error in the determination of the correction factors ξ (see Eq. (9)) for the absorption of the blue fluorescence. The fluorescence intensities were uncertain 5% to 30%, depending on He pressure (with increasing He pressure the relative error increased for infrared, and decreased for the blue fluorescence). Additionally, at He pressures <2 mbar the direct fluorescence intensity I_{917} was burdened by systematic error due to polarization effects. By checking the I_{917} intensity with polarization analyzer this error was estimated to amount to 20%. The main contribution to uncertainty of ξ (from 7% to 20% as He pressure decreased) comes from the error in the determination of the cesium ground state number density and vapor column length.

4. Conclusion

The favorable influence of the helium-induced excitation energy transfer between the cesium 6D and 7P states on the quantum efficiency of the $6S\rightarrow 6D\rightarrow 7P\rightarrow 6S$ excitation scheme has been demonstrated. This effect has resulted in a thirty-five-fold increase in the output signal of cesium resonance fluorescence detection at only moderate He pressures. As expected from theoretical investigations [21], at the pressures evaluated in this study, Ar-induced CEET was found to have little effect on the Cs RFD. The use of helium to augment the RFD response provides a practical method for increasing the resonance fluorescence detection output signal while likely minimizing radiation diffusion in imaging mode.

Acknowledgements

This research was supported by NIH Grant 63965-04 and the Ministry of Science, Education and Sport of the Republic of Croatia. T. Correll would like to thank the Institute of Physics in Zagreb for providing her with the opportunity of a working stage and for the kind hospitality.

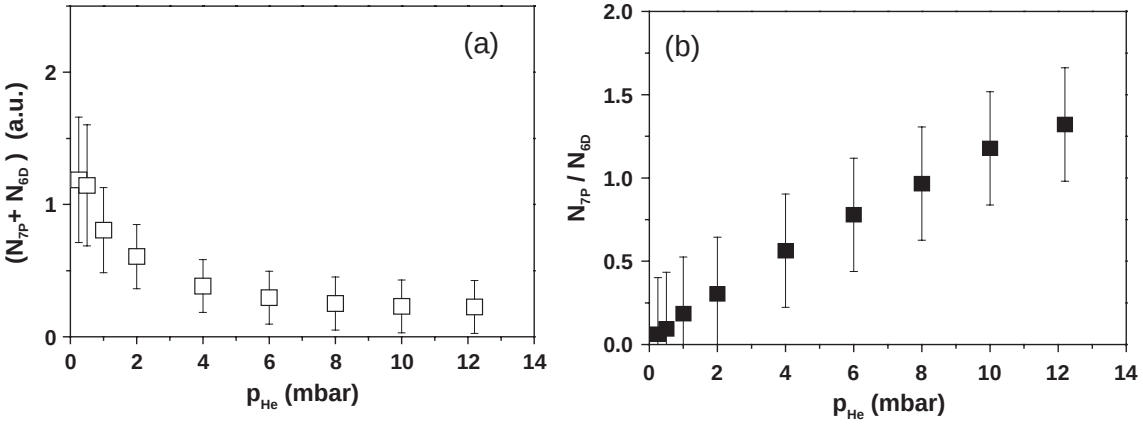

Fig. 8. (a) Total population in 7P and 6D states as a function of He pressure. (b) The population in 7P state relative to 6D population in dependence on He pressure.

References

[1] O.I. Matveev, B.W. Smith, J.D. Winefordner, Resonance ionization imaging detectors: basic characteristics and potential applications, Applied Optics 36 (1997) 8833–8843.

[2] O.I. Matveev, B.W. Smith, J.D. Winefordner, A low pressure mercury vapor resonance ionization image detector, Applied Physics Letters 72 (1998) 1673–1675.

[3] A.A. Podshivalov, W.L. Clevenger, O.I. Matveev, B.W. Smith, J.D. Winefordner, Distortion-free microchannel plate mercury atomic resonance ionization image detector, Applied Spectroscopy 54 (2000) 175–180.

[4] D. Pappas, O.I. Matveev, B.W. Smith, M.R. Shepard, A.A. Podshivalov, J.D. Winefordner, Sealed-cell mercury resonance ionization imaging detector, Applied Optics 39 (2000) 4911–4917.

[5] A.A. Podshivalov, M.R. Shepard, O.I. Matveev, B.W. Smith, J.D. Winefordner, Ultrahigh-resolution, frequency-resolved resonance fluorescence imaging with a monoisotropic mercury atom cell, Journal of Applied Physics 86 (1999) 5337–5341.

[6] J.P. Temirov, N.P. Chigarev, O.I. Matveev, N.O. Omenetto, B.W. Smith, J.D. Winefordner, A resonance ionization imaging detector based on cesium atomic vapor, Spectrochimica Acta, Part B: Atomic Spectroscopy 59 (2004) 677–687.

[7] E. Korevaar, M. Rivers, C.S. Liu, SPIE space sensing, Communications and Networking 1059 (1989) 111–118.

[8] D. Pappas, N.C. Pixley, O.I. Matveev, B.W. Smith, J.D. Winefordner, A cesium resonance fluorescence imaging monochromator, Optics Communications 191 (2001) 263–269.

[9] D. Pappas, N.C. Pixley, B.W. Smith, J.D. Winefordner, Diffusion of resonance radiation in atomic vapor imaging, Spectrochimica Acta, Part B: Atomic Spectroscopy 56 (2001) 1761–1767.

[10] D. Pappas, T.L. Correll, N.C. Pixley, B.W. Smith, J.D. Winefordner, Detection of Mie scattering using a resonance fluorescence Monochromator, Applied Spectroscopy 56 (2002) 1237–1240.

[11] N.C. Pixley, T.L. Correll, D. Pappas, O.I. Matveev, B.W. Smith, J.D. Winefordner, Tunable resonance fluorescence monochromator with sub-Doppler spectral resolution, Optics Letters 26 (2001) 1946–1948.

[12] N.C. Pixley, T.L. Correll, D. Pappas, B.W. Smith, J.D. Winefordner, Sub-Doppler spectral resolution and improved sensitivity in a cesium resonance fluorescence imaging monochromator, Applied Spectroscopy 56 (2002) 677–681.

[13] N.C. Pixley, T.L. Correll, D. Pappas, N. Omenetto, B.W. Smith, J.D. Winefordner, Moving object detection using a cesium resonance fluorescence monochormator, Optics Communications 219 (2003) 27–31.

[14] C.R. Vidal, J. Cooper, Heat-pipe oven: a new, well-defined metal vapor device for spectroscopic measurements, Journal of Applied Physics 40 (1969) 3370–3374.

[15] G.M. Grover, T.P. Cotter, G.F. Erickson, Structures of very high thermal conductance, Journal of Applied Physics 35 (1964) 1990.

[16] G.Y. Eastman, The heat pipe, Scientific American 218 (1968) 38–46.

[17] J.B. Taylor, I. Langmuir, Vapor pressure of caesium by the positive ion method, Physical Review 51 (1937) 753–760.

[18] A.N. Nesmeyanov, in: R. Gray (Ed.), Vapor Pressure of the Chemical Elements, Elsevier, Amsterdam, 1963.

[19] W. Hansen, The application of polarisation-influenced Thomas–Fermi ion models to alkali-atom transitions, Journal of Physics. B, Atomic, Molecular and Optical Physics 17 (1984) 4833–4850.

[20] P.M. Stone, Cesium oscillator strengths, Physical Review 127 (1962) 1151–1156.

[21] C. Vadla, V. Horvatic, K. Niemax, Radiative transport and collisional transfer of excitation energy in Cs vapors mixed with Ar or He, Spectrochimica Acta, Part B: Atomic Spectroscopy 58 (2003) 1235–1277.

[22] T.L., Correll, V., Horvatic, N., Omenetto, J.D., Winefordner, to be submitted to Spectrochim. Acta Part B.

[23] A. Thorne, U. Litzén, S. Johanson, Spectrophysics—Principles and Applications, Springer Verlag, Berlin, 1999.

[24] F. Siegling, K. Niemax, Low-pressure noble gas broadening of the Cs resonance lines, Zeitschrift für Naturforschung 39a (1984) 447–454.

[25] Z.J. Jabbour, J. Sagle, R.K. Namiotka, J. Huennekens, Measurement of the self-broadening rate coefficients of the cesium resonance lines, Journal of Quantitative Spectroscopy & Radiative Transfer 54 (1995) 767–778.

[26] W.E. Baylis, Collisional depolarization in the excited state, in: W. Hanle, H. Kleinpoppen (Eds.), Progress In Atomic Spectroscopy—Part B, Plenum Press, New York, 1978, pp. 1227–1297.

[27] C. Vadla, K. Niemax, J. Brust, Energy pooling in cesium vapor, Zeitschrift für Physik D 37 (1996) 241–247.

[28] V. Horvatic, M. Morre, C. Vadla, Temperature dependence of the cross section for the energy pooling process Na(3P) + Na(3P) → Na(4D) + Na(3S), Journal of Physics B: Atomic Molecular and Optical Physics 32 (1999) 4959–4976.